Co., San Fernando, California.

References

Basinger, S., Bok, D., & Hall, M. (1976) *J. Cell Biol. 69*, 29–42.
Bownds, D., Dawes, J., Miller, J., & Stahlman, M. (1972) *Nature (London), New Biol. 237*, 125–127.
Chader, G. J., Fletcher, R. T., & Krishna, G. (1975) *Biochem. Biophys. Res. Commun. 64*, 535–538.
Chader, G. J., Fletcher, R. T., O'Brien, P. J., & Krishna, G. (1976) *Biochemistry 15*, 1615–1620.
Corbin, J. D., Keely, S., & Park, C. R. (1975) *J. Biol. Chem. 250*, 218–225.
Farber, D. B., & Lolley, R. N. (1973) *J. Neurochem. 21*, 817–828.
Fletcher, R. T., & Chader, G. J. (1976) *Biochem. Biophys. Res. Commun. 70*, 1297–1302.
Frank, R. N., & Bensinger, R. E. (1974) *Exp. Eye Res. 18*, 271–280.
Frank, R. N., & Buzney, S. M. (1975) *Biochemistry 14*, 5110–5117.
Frank, R. N., Cavanaugh, D., & Kenyon, K. R. (1973) *J. Biol. Chem. 218*, 596–609.
Goridis, C., & Weller, M. (1976) *Adv. Biochem. Psychopharmacol. 15*, 391–412.
Goridis, C., Virmaux, N., Weller, M., & Urban, P. F. (1976) *Transmitters in the Visual Process* (Bonting, S. L., Ed.) pp 27–58, Pergamon Press, Oxford.
Krishna, G., Krishnan, N., Fletcher, R. T., & Chader, G. (1976) *J. Neurochem. 27*, 717–722.
Kühn, H., Cook, J. H., & Dreyer, W. J. (1973) *Biochemistry 12*, 2495–2502.
Kühn, H., McDowell, J. H., Leser, K. H., & Bader, S. (1977) *Biophys. Struct. Mech. 3*, 175–180.
Laemmli, U. K. (1970) *Nature (London) 227*, 680–685.
Lipton, S., Rasmussen, H., & Dowling, J. (1977) *J. Gen. Physiol. 70*, 771–791.
Lolley, R. N., & Farber, D. B. (1975) *Exp. Eye Res. 20*, 585–597.
Lolley, R. N., Brown, B. M., & Farber, D. B. (1977) *Biochem. Biophys. Res. Commun. 78*, 572–578.
Lowry, O. H., Rosebrough, N. J., Farr, A. L., & Randall, R. J. (1951) *J. Biol. Chem. 193*, 265–275.
Miki, N., Keirns, J., Marcus, F., Freeman, J., & Bitensky, M. (1973) *Proc. Natl. Acad. Sci. U.S.A. 70*, 3820–3824.
Miller, J. A., & Paulsen, R. (1975) *J. Biol. Chem. 250*, 4427–4432.
Pannbacker, R. G. (1973) *Prostaglandins and Cyclic AMP* (Kahn, R. H., & Lands, W. E., Eds.) pp 251–252, Academic Press, New York.
Weller, M., Virmaux, N., & Mandel, P. (1975) *Proc. Natl. Acad. Sci. U.S.A. 72*, 381–385.
Weller, M., Virmaux, N., & Mandel, P. (1976) *Exp. Eye Res. 23*, 65–67.
Woodruff, M. L. Bownds, D., Green, S. H., Morrisey, J. L., & Shedlovsky, A. (1977) *J. Gen. Physiol. 69*, 667–669.

# Spin-Label Techniques for Monitoring Macromolecular Rotational Motion: Empirical Calibration under Nonideal Conditions†

Michael E. Johnson

ABSTRACT: Practical techniques are demonstrated for determining rotational correlation times of macromolecules from the first harmonic absorption electron spin reasonance spectra of tightly bound spin labels. The techniques are developed to compensate for such nonideal conditions as residual label motion, temperature dependence of rigid limit spectral parameters, and the presence of inhomogeneous line broadening. These effects are all shown to be of importance in monitoring the rotational motion of carbonmonoxyhemoglobin which is spin labeled with the tightly bound nitroxide label, 4-maleimido-2,2,6,6-tetramethylpiperidinyl-1-oxy. Spin-label interactions with other paramagnetic agents are also shown to produce spectral changes which are qualitatively similar to, but quantitatively different from, those resulting from increases in the rate of rotational motion.

Over the last few years there has been increasing interest in the use of spin-label techniques to monitor macromolecular motional behavior. In those favorable cases where a spin label can be rigidly bound to a macromolecule, its electron paramagnetic resonance (EPR)[1] spectrum should directly reflect the motion of the macromolecule itself. Theoretical studies by McCalley et al. (1972) and Goldman et al. (1972) have shown that in the slow motion region the apparent hyperfine splitting can be quantitatively related to the spin-label rotational correlation time. More recently Mason & Freed (1974) have predicted that the hyperfine extremal line widths should be an even more sensitive monitor for rotational motion.

Thus far, however, only the hyperfine splitting measurement method appears to have been used in monitoring macromolecular motional behavior. Through application of this technique, McConnell and co-workers have measured the rotational correlation times of spin-labeled $HbO_2$ (McCalley et al., 1972) and spin-labeled $\alpha$-chymotrypsin (Shimshick & McConnell, 1972) in solution and have shown that the spin-label measurements agree well with the behavior predicted for Brownian rotational diffusion. In an extension of this work, Kuznetsov et al. (1975) have used correlation time mea-

† From the Department of Medicinal Chemistry, College of Pharmacy, University of Illinois at the Medical Center, P.O. Box 6998, Chicago, Illinois 60680, and the Division of Biological and Medical Research, Argonne National Laboratory, Argonne, Illinois 60439. *Received August 4, 1978.* Supported in part by the Research Corporation, the National Institutes of Health (HL-15168), and the U.S. Department of Energy (at ANL).

[1] Abbreviations used: EPR, electron paramagnetic resonance; HbCO, carbonmonoxyhemoglobin; Tempo-maleimide, 4-maleimido-2,2,6,6-tetramethylpiperidinyl-1-oxy.

0006-2960/79/0418-0378$01.00/0 

surements, along with the shape asymmetry of α-chymotrypsin, to determine the orientation of the label nitroxide ring with respect to the protein matrix.

Most of the work up to the present time has assumed the tightly bound spin label to act simply as an inert reporter group for macromolecular motion, exhibiting no independent motional fluctuations and exhibiting no spectral senstivitiy to nitroxide interactions with the macromolecules. Recent work in this laboratory, however, has shown that these assumptions are not entirely valid (Johnson, 1978; M. Johnson, to be published). In Tempo-maleimide spin labeled HbCO, which has often been considered as the prime example of a protein with an immobilized spin label (McCalley et al., 1972), the nitroxide exhibits significant motional fluctuation at room temperature and above. These motional fluctuations can produce up to 0.3–0.4-G broadening of the hyperfine extremal line widths for Tempo-maleimide labeled HbCO and as much as 1–1.2-G broadening for HbCO labeled with the five-membered nitroxide ring analogue of Tempo-maleimide. Furthermore, the nitroxide interaction with the HbCO protein matrix produces a strong temperature dependence in the intrinsic rigid limit hyperfine separation. In turn, these effects can cause significant errors in correlation time calculations if corrections are not made.

The present communication describes methods for calibrating the spin-label line width and hyperfine splitting measurement techniques to accurately monitor macromolecular rotational diffusion even in the presence of such nonideal conditions as having residual label motion and substantial temperature dependence of the label magnetic parameters. The specific advantages and limitations of each measurement method are demonstrated.

## Materials and Methods

Membrane-free HbCO was prepared and spin labeled with Tempo-maleimide by the methods described previously (Johnson, 1978). Sucrose solutions with concentrations ranging from 5% to 55% (w/v) were prepared at 5% intervals using reagent grade sucrose and glass-distilled water. HbCO–sucrose solutions for variable viscosity studies were then prepared by adding desalted 30–35% HbCO to the sucrose solutions in a ratio of 1:10 to give a final HbCO concentration of approximately 3%. Solution viscosities were calculated from the empirical relations of Barber (1966). Immobilized HbCO samples were prepared by combining labeled and unlabeled HbCO in a molar ratio of 1:2 and precipitating the resulting solution with saturated (at 4 °C) ammonium sulfate at pH 7.

The effects of additional paramagnetic agents upon the EPR spin-label spectra were studied by adding aliquots of 0.5 M $NiCl_2$ in Tris buffer, pH 7.0, to desalted HbCO solutions. Concentrations were adjusted to maintain a constant HbCO concentration of 9.1 g/dL with increasing Ni concentration. Temperature was held constant at 1.4 °C during spectral measurements.

Spin-label EPR spectra were measured on a Varian E-112 spectrometer equipped with an E-257 variable temperature accessory. A microwave power of 5 mW was found to introduce no observable saturation line broadening at temperatures above 0 °C and was used for all measurements unless otherwise noted. No perceptible line broadening was observed at a modulation level of 1 G; thus this modulation amplitude was used at all temperatures.

Line widths and hyperfine separations were measured using 40 and 100 G sweep widths, respectively. Sweep widths were calibrated from the tetracyanoethylene anion in dimethoxyethane (Polnaszek, 1976) and from the residual $Mn^{2+}$ in SrO (Bolton et al., 1972). Temperature was measured using a copper–constantin thermocouple and a Honeywell Model 2746 potentiometer. The relative precision of any one measurement with respect to another measurement is estimated to be approximately ±0.5 °C; the absolute accuracy of individual measurements is estimated to be approximately ±1 °C. Samples were contained in 50 or 100 μL sealed glass capillary pipettes and were held in the cavity by a specially constructed holder.

Line widths were measured by shifting the field off resonance, determining the base line, and then measuring the full line width at half-maximum with respect to the base line. Plotted values of both the line widths and the hyperfine separations are the average of two measurements.

Numerical values for the parameters of the various equations were derived by nonlinear least-square methods using the nonlinear routines of the SAS package (Barr et al., 1976).

## Results and Discussion

*Spectral Parameterization.* From Figure 1 it can be seen that the apparent hyperfine splitting decreases substantially, both as the rate of rotational motion increases, and as the temperature increases. Goldman et al. (1972) have shown that the rotational correlation time can be related to the apparent hyperfine splitting, $A_{zz}$*, by the expression

$$\tau_R^{-1} = a_z\left(1 - \frac{A_{zz}^*}{A_{zz}^0}\right)^{b_z} \quad (1)$$

where $\tau_R$ is the rotational correlation time, $a_z$ and $b_z$ are parameters derived from spectral simulation, and $2A_{zz}^0$ is the true hyperfine splitting in the absence of motion (i.e., the rigid limit splitting). In the use of this equation, most workers have assumed that the parameters $a_z$, $b_z$, and $A_{zz}^0$ are independent of temperature, and that the label is completely motionless with respect to any macromolecular matrix. To correct for such effects we use an empirical method for correlating $\tau_R$ with $A_{zz}$. For solutions of known temperature and viscosity the Stokes relation

$$\tau_R = \frac{4\pi r^3 \eta}{3kT} \quad (2)$$

may be used to directly calculate the Hb rotational correlation time where $r$ is the effective Hb radius, $\eta$ is the solvent viscosity, $k$ is Boltzmann's constant, and $T$ is absolute temperature. Substituting this expression into eq 1 then permits us to empirically relate the apparent splitting, $2A_{zz}$*, to $\tau_R$ even in the presence of such nonideal labeling conditions as residual label motion or temperature-dependent parameters.

Spin-labeled HbCO samples with differing viscosities were prepared by dissolving the labeled HbCO into sucrose solutions of different concentrations as described above. The values of $2A_{zz}$* for these samples were then measured from the EPR spectra at the three temperatures, 4.5, 25, and 45 °C, and the inverse correlation times ($\tau_R^{-1}$) calculated from eq 2. Figure 2 shows the relationship between $\tau_R^{-1}$ and $2A_{zz}$* at the three different temperatures and demonstrates the existence of a strong intrinsic temperature dependence in the apparent hyperfine separations. Equation 1 was fit to the data of Figure 2, allowing all three parameters $a_z$, $b_z$, and $A_{zz}^0$ to vary. The exponent, $b_z$, was found to be independent of temperature. However the rigid limit splitting, $2A_{zz}^0$, and the "slope" parameter, $a_z$, both exhibit substantial temperature dependence. The various values and their uncertainties are given in Table IA.

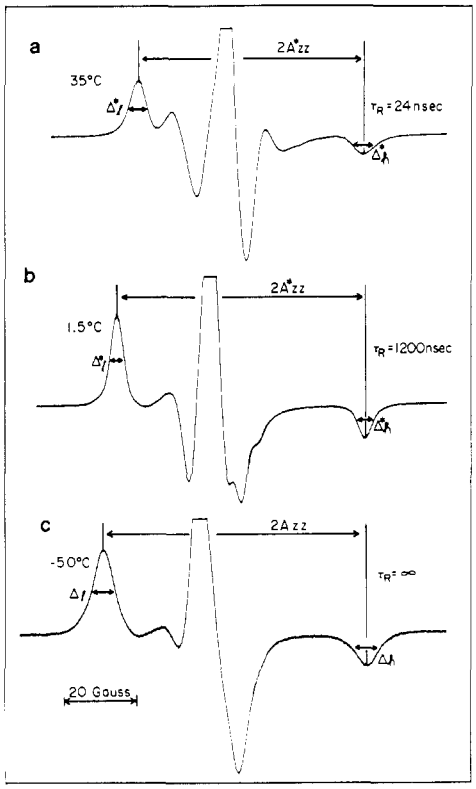


FIGURE 1: Tempo-maleimide spin-labeled HbCO spectra under various solution conditions. (a) Hb solution, 9.1%, in distilled water at 35 °C; (b) 7.2% HbCO in ~45% sucrose at 1.5 °C; and (c) 9.1% HbCO frozen in distilled water at −50 °C. Note that the hyperfine separation, $2A_{zz}$, decreases both as temperature is increased (compare the frozen Hb spectrum at −50 °C (c) with the nearly immobilized one at 1.5 °C (b)), and as the rate of rotational motion increases (spectra a and b). The hyperfine line widths, $\Delta_l$ and $\Delta_h$, increase rapidly as the rate of rotational motion increases (spectra a and b), but also increase due to intrinsic broadening mechanisms for very slow rotational motion or for complete immobilization (compare c with b and a). Correlation times shown are calculated from eq 8–10 as described in the text. $\tau_R$ for a is a weighted average (Wang et al., 1975) of the values calculated from all three of the spectral parameters. Intrinsic broadening mechanisms affect both line widths in (b); thus the correlation time is calculated from only the apparent hyperfine separation (eq 8).

The temperature dependence of the rigid limit splitting is shown in Figure 3. Parameterizing this dependence in the form

$$A_{zz}^{0}(T) = c + d/T \text{ (K)} \quad (3)$$

gives the straight (solid) line in Figure 3, from which it can be seen that $A_{zz}^{0}$ exhibits a nearly perfect $1/T$ dependence over the temperature range 3 to 45 °C. This strong temperature dependence appears to result from hydrogen bond formation between the N–O group of Tempo-maleimide and a proton donor within the Tempo-maleimide binding site (M. Johnson, to be published). Small amplitude librational motion of the label may also contribute to this behavior (Johnson, 1978).

We have also studied the temperature dependence of the rigid limit hyperfine separation, $2A_{zz}^{0}$, under conditions where the HbCO molecules were directly immobilized by precipitation in ammonium sulfate. These data are also shown in Figure 3. In comparing these two sets of data, it is clear that the temperature behavior of the rigid limit splitting is strongly dependent on the mechanism of protein immobilization. The splittings obtained from HbCO precipitated in saturated ammonium sulfate exhibit a substantially flatter temperature slope (dashed line) than do those obtained by viscosity extrapolation. The viscosity extrapolation technique is preferred for this parameterization since the sucrose solutions would be expected to more closely approximate the native protein environment than would saturated ammonium sulfate.

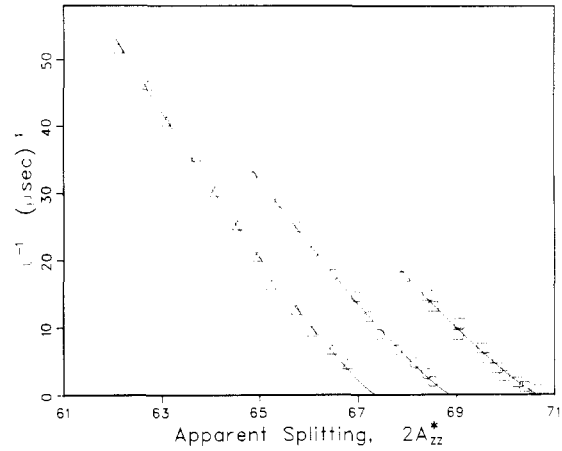


FIGURE 2: Correlation time calibration of the hyperfine separation, $2A_{zz}^*$. The symbols □, ○, and △ denote the values of $2A_{zz}^*$ as measured at 4.5, 25, and 45 °C, respectively. Measurement accuracy is approximately ±0.3 G. $\tau_R^{-1}$ is calculated from the Stokes relation (eq 2) using a value of 32.3 Å for the HbCO radius (Alpert & Banks, 1976) and calculating the viscosity from the relations of Barber (1966). The solid lines shown are the parameterization of eq 1, derived by least-square methods as described in the text.

Table I: Spectral Parameterizations

A. hyperfine separation regression[a]

| $T$ (°C) | $2A_{zz}^{0}$ (G) | $a_z$ ($10^8$ s$^{-1}$)[b] | $b_z$ |
|---|---|---|---|
| 4.5 | 70.64 ± 0.08 | 8.57 ± 1.34 | 1.18 ± 0.05 |
| 25 | 68.90 ± 0.09 | 9.58 ± 1.24 | 1.18 ± 0.05 |
| 45 | 67.34 ± 0.11 | 10.87 ± 1.22 | 1.18 ± 0.05 |

B. line width regression[c]

| $T$ (°C) | $m$ | $\Delta_m^{0}$ (G) | $a_m$ ($10^6$ s$^{-1}$) | $b_m$ |
|---|---|---|---|---|
| 3.2 | $l$ | 4.04 ± 0.02[d] | 112.5 ± 3.7 | 0.906 ± 0.042 |
| 24.8 | $l$ | 4.06 ± 0.03[d] | 112.5 ± 3.7 | 0.906 ± 0.042 |
| 44.6 | $l$ | 4.24 ± 0.03 | 112.5 ± 3.7 | 0.906 ± 0.042 |
| 3.2 | $h$ | 4.20 ± 0.13 | 65.6 ± 5.1 | 1.43 ± 0.10 |
| 24.8 | $h$ | 4.32 ± 0.14 | 65.6 ± 5.1 | 1.43 ± 0.10 |
| 44.6 | $h$ | 4.51 ± 0.14 | 65.6 ± 5.1 | 1.43 ± 0.10 |

[a] The values listed here are the result of a nonlinear regression in which $A_{zz}^{0}$ and $a_z$ were allowed to assume independent values at each temperature, but the exponent, $b_z$, was required to maintain a single value independent of temperature. Allowing $b_z$ to assume independent values at each temperature yielded values which were equivalent within the statistical uncertainty. Thus the regressions were linked to yield a single, temperature independent, value for $b_z$. [b] The large uncertainty in this parameter reflects extreme sensitivity to the value of the exponent, $b_z$. If $b_z$ is held constant and a two-parameter regression is used to determine $A_{zz}^{0}$ and $a_z$, the uncertainty in $a_z$ is reduced by approximately an order of magnitude. [c] The values listed here are the results of nonlinear regressions in which $\Delta_m^{0}$ was allowed to assume independent values at each temperature, but the exponent, $b_m$, and the "slope", $a_m$, were required to maintain single values independent of temperature. Regressions for the low-field and high-field lines were completely independent of each other. [d] The values of $\Delta_l^{0}$ at 3 and 25 °C are statistically equivalent, but have been considered separately for consistency with treatment of high-field line-width temperature dependence.

The behavior of the linear coefficient or "slope" parameter, $a_z$, is almost perfectly linear with temperature, and can best be described as a straight line of the form

$$a_z(T) = a_0 + a_1 T \quad (4)$$

Substituting $A_{zz}^{0}(T)$ (eq 3) and $a_z(T)$ (eq 4) into eq 1 then generates the solid calculated curves shown in Figure 2. From a comparison of the calculated curves with the experimental

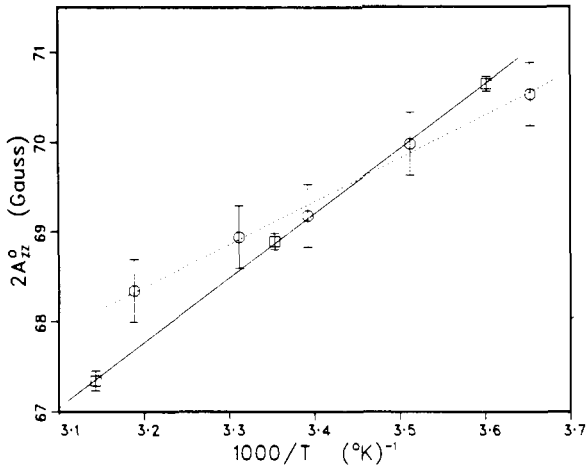


FIGURE 3: Temperature dependence of the rigid limit hyperfine separation, $2A_{zz}^0$. The symbols □ and ○ denote values as determined by viscosity extrapolation and ammonium sulfate precipitation, respectively. Error bars for the ammonium sulfate precipitation data are the estimated uncertainties of the individual measurements; the viscosity extrapolation error bars are the standard errors of estimate from the regressions. Both data sets follow a $1/T$ dependence quite closely, but exhibit substantially different slopes. The solid line is from the least-squares regression of the viscosity extrapolated data; the dashed line is from the regression of the ammonium sulfate precipitated HbCO data. The viscosity extrapolation procedure is considered preferable as the method for determining the rigid limit hyperfine separation since it reproduces physiological conditions more closely than does saturated ammonium sulfate.

data in this figure, it can be seen that this parameterization fits the original data quite well, with no apparent systematic discrepancies. These equations and the relevant parameters are summarized for convenience in Table IIA.

From the spectra in Figure 1 it can also be seen that both the low-field and high-field hyperfine extremal line widths increase substantially as the rate of rotational motion increases (spectra a and b). Mason & Freed (1974) have shown that $\tau_R$ can also be related to the hyperfine line widths by the expression

$$\tau_R^{-1} = a_m\left(\frac{\Delta_m^*}{\Delta_m^0} - 1\right)^{b_m}, \quad m = l, h \qquad (5)$$

Table II: Final Parameterization Equations

A. hyperfine separation

$$\tau_R^{-1} = a_z(T)\left(1 - \frac{A_{zz}^*}{A_{zz}^0(T)}\right)^{1.18} \quad (10^6\ s^{-1})$$

$a_z(T) = 826 + 5.68T\ (°C) \times (10^6\ s^{-1})$

$2A_{zz}^0(T) = 44.7 + 7200/T(K)\ (G)$

B. line widths

$$\tau_R^{-1} = a_m\left(\frac{\Delta_m^*}{\Delta_m^0(T)} - 1\right)^{b_m}$$

$a_l = 1.125 \times 10^8\ s^{-1}$, $b_l = 0.906$

$\Delta_l^0(T) = 4.038 + (5.564 \times 10^{13})\ \exp(-10560/T\ (K))\ (G)$

$a_h = 6.56 \times 10^7\ s^{-1}$, $b_h = 1.43$

$\Delta_h(T) = 4.11 + 7580\ \exp(-3134/T\ (K))\ (G)$

where $a_m$ and $b_m$ are parameters derived from spectral simulation, $\Delta_m^0$ are the hyperfine line widths in the absence of motion, $\Delta_m^*$ are the hyperfine line widths in the presence of motion, and $m$ is the index referring to either the low-field ($\Delta_l$) or high-field ($\Delta_h$) lines.

Measuring the values of $\Delta_m^*$ as a function of $\tau_R$ at the three temperatures 5, 25, and 45 °C then gives the data shown in Figure 4. Equation 5 was fit to these data, allowing the three parameters $a_m$, $b_m$, and $\Delta_m^*$ to vary for each of the hyperfine lines (i.e., the regressions for the low-field and high-field lines were done independently). For very slow rotational times ($\tau_R^{-1} < 3.5\ \mu s^{-1}$), the line widths appear to increase again as the rate of rotational motion decreases. (See particularly the low-field line width inset in Figure 4.) For this reason, only the relatively rapid motion data ($\tau_R^{-1} > 3.5\ \mu s^{-1}$) were used in the parameterizations. The exponents, $b_m$, and the parameters, $a_m$, exhibited no apparent temperature dependence. The rigid limit line widths, $\Delta_l^0$ and $\Delta_h^0$, however, both exhibit a significant degree of temperature dependence as shown in Table IB.

It should be noted that the rigid limit line widths also depend strongly on the technique used to measure them. Freezing the HbCO solution provides a more direct technique for immobilizing the HbCO molecule than does the viscosity extrapolation. However, from Figure 1 it can be seen that the hyperfine line widths in the frozen solution (−50 °C) are even broader than those of the HbCO solution at 35 °C and are

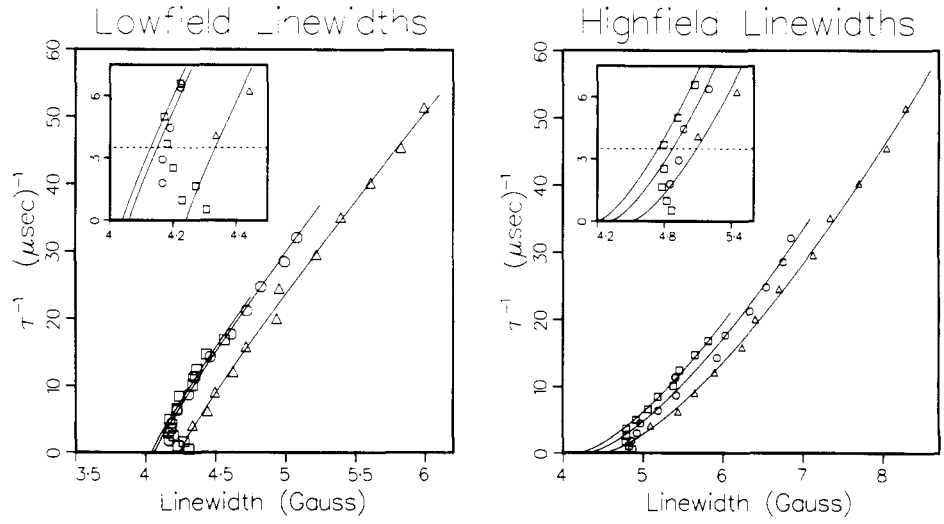


FIGURE 4: Correlation time calibration of the hyperfine line widths, $\Delta_l^*$ and $\Delta_h^*$. The symbols □, ○, and △ denote the line width values as measured at 3, 25, and 45 °C, respectively. Measurement accuracy is approximately ±0.05 G for $\Delta_l^*$ and ±0.1 G for $\Delta_h^*$. $\tau_R^{-1}$ is calculated as described for Figure 2. The solid lines shown are the parameterizations of eq 5, derived by the least-square methods given in the text. The insets show an expanded view of the very slow motion data. The deviation of the slow motion ($\tau_R^{-1} < 3.5 \times 10^6\ s^{-1}$) data from the parameterization lines is apparently due to intrinsic broadening mechanisms.

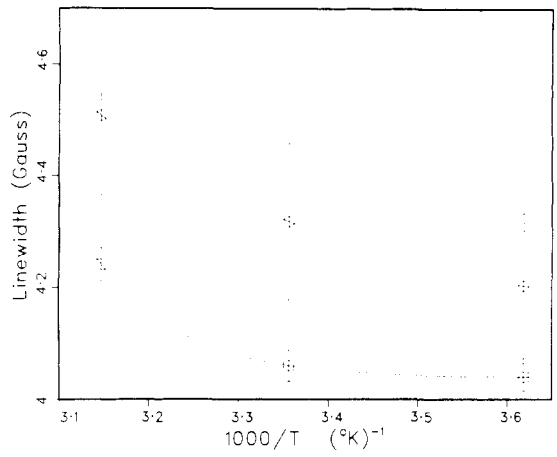


FIGURE 5: Temperature dependence of the viscosity extrapolated rigid limit line widths. The symbols □ and ○ denote the values of $\Delta_l^0(T)$ and $\Delta_h^0(T)$, respectively. Error bars are the standard estimates of error. The solid lines are the solutions to eq 6.

substantially broader than those of the HbCO–sucrose solution at 1.5 °C. The most plausible sources for this "excess" line broadening in frozen HbCO are electron–nuclear hyperfine interactions between the electron and the protons of the spin label and its host and heterogeneity of the spin-label environment within the HbCO molecule (Freed, 1976). These mechanisms will be referred to hereafter as "intrinsic broadening mechanisms", to distinguish them from motionally induced broadening or paramagnetically induced broadening. Freed (1976) has noted that much of this intrinsic broadening will be rapidly averaged with the onset of molecular motion. Thus it is probably also these intrinsic broadening mechanisms which produce the increases in line width at very slow rotational rates ($\tau_R < 3.5\ s^{-1}$) as seen in the insets of Figure 4. This suggests that the viscosity extrapolation effectively permits averaging of some of the intrinsic broadening interactions, while freezing the solution provides a truly immobilized protein with all of the intrinsic broadening mechanisms present. The viscosity extrapolation technique for measuring these parameters would thus appear to be the most appropriate since correlation time measurements will necessarily be made in the presence of rotational motion.

The temperature behavior of the viscosity extrapolated rigid limit line widths is shown in Figure 5, where it can be seen that the dependence is distinctly nonlinear. This change in rigid limit line width has previously been shown to be the result of residual label motion within the Hb label binding site (Johnson, 1978). Since the line width increase is the result of a thermally induced increase in the amplitude and/or frequency of librational motion, we might expect the line-width temperature behavior to follow the general form

$$\Delta_m^0(T) = f_m + g_m e^{-\kappa_m/T},\ m = l,\ h \qquad (6)$$

The appropriate solutions to this equation (i.e., the values of the parameters $f_m$, $g_m$, and $\kappa_m$) were calculated from the $\Delta_m^0$ data (Table IB) and are shown as the solid lines in Figure 5. The quality of fit for this equation is not estimated since the three data points provide an exact solution to the three-parameter equations.

Substituting eq 6 into eq 5 then generates the solid lines shown in Figure 4. From this figure it can be seen that these parameterizations fit the original data quite well for values of $\tau_R^{-1} \gtrsim 3.5\ \mu s^{-1}$. For very slow rotational motion, where $\tau_R^{-1} \lesssim 3.5\ \mu s^{-1}$, the intrinsic broadening begins to appear and the parameterizations are no longer accurate.

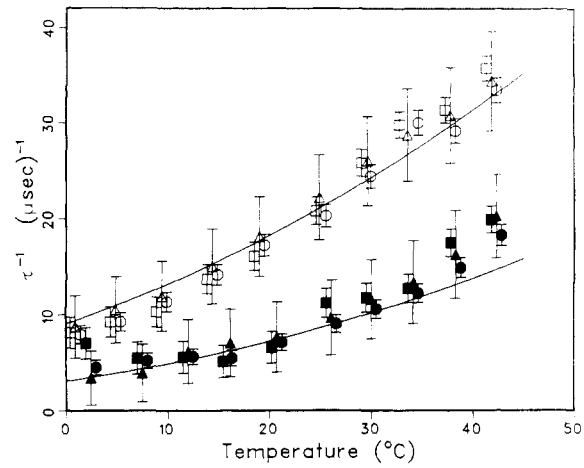


FIGURE 6: Temperature comparison of Hb rotational rates calculated from spectral parameters with the Stokes relation. The symbols □, ○, and △ denote values of $\tau_R^{-1}$ as calculated from $\Delta_l^*$, $\Delta_h^*$, and $2A_{zz}^*$, respectively. The upper (open symbols) and lower (solid symbols) data sets correspond to samples of 3% HbCO in 14.4% and 33.3% sucrose, respectively. The solid lines are calculated from the Stokes relation (eq 2). The $\tau_R^{-1}$ values as calculated from $\Delta_l^*$ and $\Delta_h^*$ are respectively offset by −0.5 and +0.5 °C from their true temperatures to prevent overlap of error bars.

In comparing the relative precision of each of the parameterizations, the approximate uncertainties, $\delta(1/\tau_R)$, in the calculated values of $1/\tau_R$ are

$$\delta_m(1/\tau_R) \simeq a_m \frac{\delta(\Delta_m^*)}{\Delta_m^0},\ m = l,\ h \text{ (line widths)} \qquad (7a)$$

$$\delta_z(1/\tau_R) \simeq a_z \frac{\delta(A_{zz}^*)}{A_{zz}^0} \text{ (hyperfine separation)} \qquad (7b)$$

where $\delta(\Delta_m^*)$ and $\delta(A_{zz}^*)$ are respectively the measurement uncertainties of the hyperfine line widths and hyperfine separation. Assuming measurement uncertainties similar to those of the data in Figures 2 and 4 gives uncertainties of $\delta(1/\tau_R) \sim \pm 1$, 1.5, and 3–5 $\mu s^{-1}$ for the high-field line-width, low-field line-width, and hyperfine separation calculations, respectively. The high-field line-width calculation thus appears to offer the highest precision, followed in order by the low-field line-width and the hyperfine separation calculations. A weighted average of these calculations should then give the best value. (For relatively slow motion, however, the line-width and hyperfine separation calculations should be compared to ensure that intrinsic broading mechanisms are not producing errors.)

*Test Comparisons.* In order to test the validity of our parameterizations of the above temperature dependencies, we compare the temperature dependence of HbCO rotational rates as determined from the EPR spectra with the rates as predicted by the Stokes relation (eq 2). The upper and lower curves in Figure 6 are from 3% HbCO in 14.4% and 33.3% sucrose solutions, respectively. It can be seen that the three parameterizations are quite consistent with each other; the calculated values of $1/\tau_R$ overlap within calculated uncertainty for all except one of the temperature/viscosity measurements. This discrepancy occurs at ~2.4 °C for the 33% sucrose solution where the low-field line-width calculation gives a value of $\tau_R^{-1}$ significantly higher than that of the other two calculations. This discrepancy apparently results from the increased intrinsic broadening which appears at slow rotational rates. This emphasizes the necessity of checking the different calculations for consistency. The spectral calculations also appear to agree quite well with the rotational behavior pre-

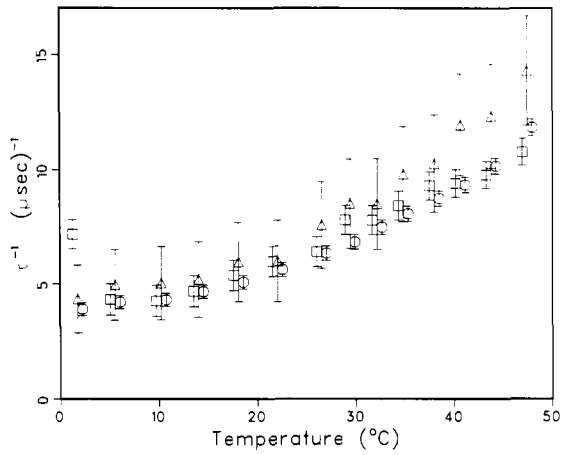


FIGURE 7: Temperature comparison of the Hb rotational rates as calculated from the different spectral parameterizations. The symbols □, O, and Δ denote values of $\tau_R^{-1}$ as calculated from $\Delta_l$*, $\Delta_h$*, and $2A_{zz}$*, respectively. Error bars result from measurement uncertainty only and do not include any effects from the parameterizations themselves. The $\tau_R^{-1}$ values as calculated from $\Delta_l$* and $\Delta_h$* are respectively offset by −0.5 and +0.5 °C from their true temperatures to prevent overlap of error bars.

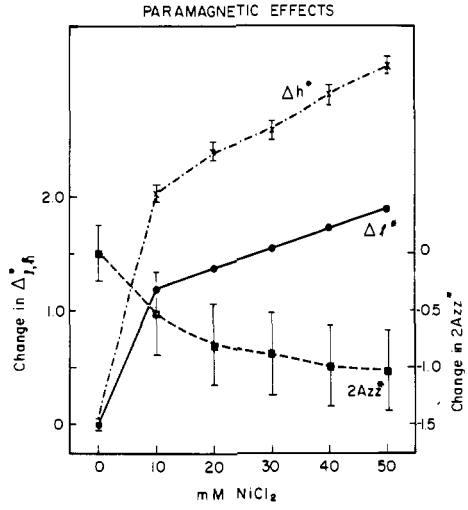


FIGURE 8: Spectral effects of paramagnetic agents. The left vertical axis denotes the increase in $\Delta_l$* and $\Delta_h$* as Ni concentration increases; the right vertical axis denotes the corresponding decrease in $2A_{zz}$*. The Hb samples were desalted and held at a constant 9.1% concentration at 1.4 °C.

dicted by the Stokes equation (the solid lines in Figure 6). The only significant discrepancy occurs for high temperature ($T$ > 40 °C) measurements with the 33% sucrose solution, where the spectral calculations suggest a slightly more rapid rate of rotational motion than is predicted by the Stokes relation. This discrepancy probably has little practical importance, however, since few measurements would be made at such high temperatures due to problems of thermal denaturation.

The temperature dependence of rotational motion in a concentrated HbCO solution, shown in Figure 7, gives us a further comparison of the parameterization methods. Again we see that the low-field line-width calculation gives us a $\tau_R^{-1}$ value which is anomalously large for slow motion at low temperature. There also appears to be some difference in the rotational rate as predicted from the hyperfine separation and from the line widths. From approximately 5 to 35 °C, the hyperfine separation suggests a very slightly higher rotational rate than does either of the line widths; at about 40 °C and above the disagreement between the two methods becomes fairly substantial, with the hyperfine separation giving $\tau_R^{-1}$ values ~20% larger than those from the line widths. This discrepancy may be due to differing solution conditions between the buffered HbCO solution and the desalted sucrose solutions in which the parameterizations were done. We have previously shown that the magnitude of line broadening due to librational motion is sensitive to solution ionic strength (Johnson, 1978). Thus the 0.05 M phosphate buffer in the concentrated HbCO solution may be reducing the librational broadening. Reducing the librational broadening in the $\Delta_m^0(T)$ parameters of eq 5 by ~30% (~0.15 G) would, in fact, be sufficient to give agreement over the full temperature range. It is also possible that the solution ionic strength may affect the hyperfine separation. However, one would expect such an effect to produce a decrease in the $\tau_R^{-1}$ calculations when compared with the line-width calculations, rather than an apparent increase as seen here. Although the high temperature data demonstrate the existence of a discrepancy between the different calculations, the discrepancy is fairly small over reasonable temperature ranges (0 to about 38 °C) and thus is probably not too important for practical measurements.

*Paramagnetic Effects.* In some applications it may be desirable to measure macromolecular rotational rates in the presence of paramagnetic agents. An example of the effects of such an agent upon the spin-label spectral behavior is shown in Figure 8. From this figure it can be seen that the $\Delta_m$* increase substantially, while $A_{zz}$* decreases to a somewhat smaller extent in the presence of $NiCl_2$. The rapid change in these parameters between 0 and 10 mM $NiCl_2$ concentration may indicate the presence of an Hb–Ni binding site near the β93 spin-label location. The change in all of these parameters is in the same direction as would be observed for a substantial increase in rotational motion. For low concentrations of paramagnetic species, where the line-width and splitting changes are small, it would thus be fairly easy to confuse paramagnetic effects with changes in rotational rate. Oxygen, in particular, would be one of the most important sources of such error. Under atmospheric conditions oxygen appears to produce ~0.1–0.2 G line broadening. Even these small changes can be of significance for very detailed comparisons of motional states.

However, at relatively higher paramagnetic species concentration, the rotational rate calculations using the parameterizations described above would give conflicting results from the different parameters. Therefore, by use of the methods presented here, it may be possible to identify paramagnetic effects and make appropriate corrections for calculating motional rates from such data.

## Conclusions

We have studied the temperature dependence of several spectral parameters of a spin label tightly bound within a macromolecule, both in viscous media and in precipitated form, and have developed the parameterization techniques described above to provide a simple and fairly straightforward method for using spin labels to study rotational motion in macromolecular systems.

The rate of rotational motion has been shown to be related to the apparent hyperfine separation and to the hyperfine extremal line widths by the following three equations:

$$\tau_R^{-1} = a_z(T)\left(1 - \frac{A_{zz}^*}{A_{zz}^0(T)}\right)^{b_z} \quad (8)$$

$$\tau_R^{-1} = a_l\left(\frac{\Delta_l^*}{\Delta_l^0(T)} - 1\right)^{b_l} \quad (9)$$

$$\tau_R^{-1} = a_h\left(\frac{\Delta_h^*}{\Delta_h^0(T)} - 1\right)^{b_h} \quad (10)$$

The basic forms of these equations have been taken from the theoretical calculations of Goldman et al. (1972) and Mason & Freed (1974). The temperature dependencies of the parameters $a_z(T)$, $A_{zz}^0(T)$, $\Delta_l^0(T)$, and $\Delta_h^0(T)$ were obtained by basically a two-step process, first extrapolating the hyperfine separation and extremal line widths to infinite viscosity to obtain numerical values for their rigid limit values, and for the "slope" parameters, $a_z$, $a_l$, and $a_h$. Linear and exponential equations were then used to develop empirical relationships for the temperature dependencies of the various parameters. The appropriate values are summarized in Table II.

Of the three spectral parameters, the high-field line width, $\Delta_h^*$, appears to be most sensitive to rotational motion. However, it also appears to be the parameter most sensitive to librational motion and thus requires a careful determination of the rigid limit line-width temperature dependence, $\Delta_h^0(T)$. The low-field line width, $\Delta_l^*$, is easier to measure in dilute samples due to its narrower width (and thus, better signal-to-noise ratio) and appears to be somewhat less affected by librational motion. However, it is also less sensitive to intrinsic broadening mechanisms than the high-field line width. The hyperfine separation, $2A_{zz}^*$, has the disadvantages of being substantially less sensitive to rotational motion than either of the line widths, and of being highly temperature dependent. On the other hand, it does have the advantages of apparently being unaffected by intrinsic broadening mechanisms and of being less sensitive to librational motion and paramagnetic interaction effects than either of the line widths. Thus, for measuring rotational motion, the line widths provide the most sensitive monitors, with the hyperfine separation also valuable as a consistency check for the presence of intrinsic broadening, librational motion, or paramagnetic interaction effects. Deuteration of the nitroxide ring should substantially improve both the sensitivity and accuracy of measurements in the slow motion region.

Deriving the various parameters through viscosity extrapolation is somewhat tedious, but has the advantage over other methods that it yields values appropriate to experimental solution conditions. For more accurate parameterizations it would probably also be advantageous to use buffered solutions, rather than using distilled water–sucrose solutions. This would permit the standardization to be done under ionic strength conditions similar to those of the experiment of interest.

The methods outlined here are particularly useful for comparative studies and have recently been shown to be sufficiently sensitive to detect sickle Hb aggregation even in the fully carbonmonoxyheme-liganded state (Johnson & Danyluk, 1978). Other applications are in progress. Work is also in preparation to adapt these methods to nonspherical systems where anisotropic motion will be of importance.

Acknowledgments

I thank Dr. Steven S. Danyluk for providing very generous access to facilities in his laboratory at Argonne National Laboratory.

References

Alpert, S. S., & Banks, G. (1976) *Biophys. Chem. 4*, 287–296.
Barber, E. J. (1966) *Natl. Cancer Inst., Monogr. 21*, 219–239.
Barr, A. J., Goodnight, J. H., Sall, J. P., & Helwig, J. T. (1976) *A User's Guide to SAS76*, Sparks Press, Raleigh, NC.
Bolton, J. R., Borg, D. C., & Swartz, H. M. (1972) in *Biological Applications of Electron Spin Resonance* (Swartz, H. M., Bolton, J. R., & Borg, D. C., Eds.) pp 63–118, Wiley-Interscience, New York.
Freed, J. H. (1976) in *Spin Labeling Theory and Applications* (Berliner, L. J., Ed.) pp 53–132, Academic Press, New York.
Goldman, A. A., Bruno, G. V., & Freed, J. H. (1972) *J. Phys. Chem. 76*, 1858–1860.
Johnson, M. E. (1978) *Biochemistry 17*, 1223–1228.
Johnson, M. E., & Danyluk, S. S. (1978) *Biophys. J. 24*, 517–524.
Kuznetsov, A. N., Ebert, B., & Gyul'khandanyan, G. V. (1975) *Mol. Biol. (Engl. Transl.) 9*, 697–703.
Mason, R. P., & Freed, J. H. (1974) *J. Phys. Chem. 78*, 1321–1323.
McCalley, R. C., Shimshick, E. J., & McConnell, H. M. (1972) *Chem. Phys. Lett. 13*, 115–119.
Polnaszek, C. F. (1976) Dissertation, Cornell University, Ithaca, NY.
Shimshick, E. J., & McConnell, H. M. (1972) *Biochem. Biophys. Res. Commun. 46*, 321–327.
Wang, C. H., Willis, D. L., & Loveland, W. D. (1976) *Radiotracer Methodology in the Biological, Environmental, and Physical Sciences*, p 306, Prentice-Hall, Englewood Cliffs, NJ.